Journal of Marine Systems 163 (2016) 12–22

Contents lists available at ScienceDirect

Journal of Marine Systems

journal homepage: www.elsevier.com/locate/jmarsys

# Time series analysis of data for sea surface temperature and upwelling components from the southwest coast of Portugal

Priscila Costa Goela [a,b,*], Clara Cordeiro [c,d], Sergei Danchenko [a,b], John Icely [a,e], Sónia Cristina [a,b], Alice Newton [a,f]

[a] Centro de Investigação Marinha e Ambiental (CIMA), FCT, University of Algarve, Campus de Gambelas, Faro 8005-139, Portugal
[b] Facultad de Ciencias del Mar y Ambientales, University of Cadiz, Campus de Puerto Real, Polígono San Pedro s/n, Puerto Real 11510, Cadiz, Spain
[c] Faculty of Sciences and Technology, University of Algarve, Campus de Gambelas, Faro 8005-139, Portugal
[d] Center of Statistics and Applications (CEA), University of Lisbon, Bloco C6, Piso 4, Campo Grande, 1749-016, Lisboa, Portugal
[e] Sagremarisco Lda., Apartado 21, Vila do Bispo 8650-999, Portugal
[f] NILU-IMPEC, Box 100, 2027 Kjeller, Norway

ARTICLE INFO

*Article history:*
Received 4 February 2016
Received in revised form 1 June 2016
Accepted 3 June 2016
Available online 7 June 2016

*Keywords:*
Upwelling
Sea surface temperature
Structural breaks
Spectral analysis
Iberian Peninsula
Sagres

ABSTRACT

This study relates sea surface temperature (SST) to the upwelling conditions off the southwest coast of Portugal using statistical analyses of publically available data. Optimum Interpolation (OI) of daily SST data were extracted from the United States (US) National Oceanic and Atmospheric Administration (NOAA) and data for wind speed and direction were from the US National Climatic Data Center. Time series were extracted at a daily frequency for a time horizon of 26 years. Upwelling indices were estimated using westerly ($Q_x$) and southerly ($Q_y$) Ekman transport components.

In the first part of the study, time series were inspected for trend and seasonality over the whole period. The seasonally adjusted time series revealed an increasing slope for SST (0.15 °C per decade) and decreasing slopes for $Q_x$ ($-84.01$ m$^3$ s$^{-1}$ km$^{-1}$ per decade) and $Q_y$ ($-25.20$ m$^3$ s$^{-1}$ km$^{-1}$ per decade), over the time horizon. Structural breaks analysis applied to the time series showed that a statistically significant incremental increase in SST was more pronounced during the last decade.

Cross-correlation between upwelling indices and SST revealed a time delay of 5 and 2 days between $Q_x$ and SST, and between $Q_y$ and SST, respectively. A spectral analysis combined with the previous analysis enabled the identification of four oceanographic seasons. Those seasons were later recognised over a restricted time period of 4 years, between 2008 and 2012, when there was an extensive sampling programme for the validation of ocean colour remote sensing imagery. The seasons were defined as: summer, with intense and regular events of upwelling; autumn, indicating relaxation of upwelling conditions; and spring and winter, showing high interannual variability in terms of number and intensity of upwelling events.



## 1. Introduction

Upwelling occurs in several coastal regions of the world, affecting the biological productivity and dynamics of these regions (Schwing et al., 1996). An upwelling event occurs due to the interaction between the frictional stress of wind on the ocean surface and the rotation of the earth. As a consequence, transport occurs whereby the surface water mass moves to the right (in the Northern hemisphere), and is replaced by water from beneath the surface (Lluch-Cota, 2000; Price et al., 1987). This offshore movement of surface water masses is known as Ekman transport. The cold subsurface water that reaches the euphotic zone is generally rich in nutrients, stimulating primary production. For this reason, upwelling regions account for about 20% of the global fish catch despite comprising ~1% of the coastal regions of the world (Narayan et al., 2010; Pauly and Christensen, 1994). Due to the difficulty of measuring these events directly, as well as a scarcity of long time series (Schwing et al., 1996), the assessment of upwelling events is usually performed either by measuring the phenomenon inducing agents such as wind stress and Ekman transport, or by estimating the environmental changes resulting from upwelling, such as the increase in primary productivity and the marked decline in sea surface temperature (SST)[1] (Lluch-Cota, 2000).

* Corresponding author at: CIMA, FCT, University of Algarve, ed. 7, Piso 1, Cacifo no 32, Campus de Gambelas, Faro 8005-139, Portugal.
*E-mail addresses:* priscila.goela@gmail.pt (P.C. Goela), ccordei@ualg.pt (C. Cordeiro), danchenko-sergei@tut.by (S. Danchenko), john.icely@gmail.com (J. Icely), cristina.scv@gmail.com (S. Cristina), anewton@ualg.pt (A. Newton).

[1] Abbreviation List (alphabetical order): AVHRR — Advanced Very High Resolution Radiometer; BIC — Bayesian information criterion; NOAA — National Oceanic and Atmospheric Administration; OI — Optimum Interpolation; $Q_x$ — Latitudinal component of Ekman transport, meaning upwelling conditions in the Western Coast; $Q_y$ — Longitudinal component of Ekman transport, meaning upwelling conditions in the Southern Coast; RSS — Residual Sum of Squares; SST — Sea Surface Temperature.

http://dx.doi.org/10.1016/j.jmarsys.2016.06.002

Over the last three decades, a SST data product has been made available from National Oceanic and Atmospheric Administration (NOAA) with the Optimum Interpolation (OI) 0.25 Degree Daily SST Analysis data (Reynolds et al., 2007), hereafter referred to as NOAA OI SST. This product enables a) the analysis of a large dataset, covering the recent period of global warming (Hansen et al., 2010; Lima and Wethey, 2012; Trenberth et al., 2007), and b) the possibility of comparing SST with upwelling indices based on wind stress, for a more complete characterisation of upwelling events.

The NOAA OI SST database is particularly robust, combining observations from satellite AVHRR sensors interpolated with observations from sensors on ships and buoys. Apart from global coverage at a daily resolution, it allows for the large-scale adjustments of remote sensors with respect to *in situ* data (Reynolds et al., 2007). Spurious variability has been further reduced by the continuous use of the same type of remote sensor type over the entire time series, operated from 9 different satellites (NOAA7 to NOAA19 and METOP-A) (Banzon et al., 2016). However, there are limitations due to the weakness of the bias correction in some areas, where there is limited availability of *in situ* data, especially in higher latitudes (Banzon et al., 2016). Furthermore, the SST is an aggregate of data collected over the entire day, and therefore there is no accounting for the diurnal variability (Banzon et al., 2016). Despite its limitations, the NOAA database has been one of the most used sources for global SST (e.g. Costoya et al., 2015; Girondot and Kaska, 2015; Khalil et al., 2016; Liu and Minnett, 2015; Marullo et al., 2014; Singh et al., 2013). SST is often analysed using statistical techniques for dependent data (time series).

The analysis of time series is an important and valuable approach adopted in several studies, for its ability to improve the spatial and temporal resolution of the major seasonal and inter-annual patterns in biological and oceanographic data (Vantrepotte and Mélin, 2010, 2011). These studies provide indicators about long-term changes in natural conditions, such as climate change, which is why such indicators are advised or even mandated for coastal water monitoring programmes (e.g. Water Framework Directive, 2000/60/EC) (Vantrepotte and Mélin, 2010).

### 1.1. Rationale

The Sagres region has had a significant water sampling programme for the validation of ocean colour remote sensing imagery between the end of 2008 and the beginning of 2012 (Cristina et al., 2009, 2014, 2015; Goela et al., 2013, 2014, 2015). Concurrent with satellite overpasses, the water column was sampled to use its bio-optical properties to validate satellite products in the Sagres region. Additionally, this comprehensive data set was used to derive and develop regional ocean colour algorithms. However, this development requires comprehensive knowledge of the seasonal patterns of the in-water constituents. In the case of Sagres, it has a narrow continental shelf with little influence from the coast, so that the seasons are probably better explained by changes in upwelling forcing, rather than the regular succession of calendar seasons and other underlying patterns (river discharges, winter runoffs, summer stratification, etc.) (Loureiro et al., 2005, 2011). There is a particular interest in identifying the oceanographic seasons off the Sagres region over the period of the water sampling programme related to the validation of remote sensing imagery. Indeed this time series study would provide a preliminary step in the overall characterisation of the seasonal pattern for bio-optical parameters in Sagres.

In such context, the intention was not to do a full characterisation of the upwelling process in Sagres, as this would require a robust *in situ* dataset. Instead, the study was conducted with practical and publically available databases, aiming to define oceanographic seasons by examining patterns and relationships in and between data sets for SST and upwelling indices, using statistical methodologies for dependent data. To fulfill this objective, the work was developed in three consecutive steps: 1) to conduct a preliminary analysis of the time series for SST and upwelling indices; 2) to verify the relationship between SST decreases (reflection of upwelling events) and favourable upwelling indices (forcing agents); and 3) to define the periodicity of upwelling events in the area, in order to delineate oceanographic seasons, especially during the sampling period for validation.

### 1.2. Sagres region

The study region is part of the Eastern North Atlantic Upwelling System (Wooster et al., 1976) and is located in a transition zone, where different upwelling fronts develop along the west and south of the study region.

Conditions favourable for upwelling are more intense and persistent along the west coast, induced by northerly winds, and are typically associated with summer (Fiúza et al., 1982; Loureiro et al., 2005; Relvas and Barton, 2002). Strong westerly winds can also induce occasional upwelling episodes against the typical warm counter current driven by a pressure gradient flowing along the south coast (Relvas and Barton, 2002). Upwelling filaments in the study region have been observed in satellite images for both SST and ocean colour (Fiúza, 1983; Haynes et al., 1993; Sousa and Bricaud, 1992; Sousa et al., 2008). Thus, the Sagres study site, located at 2 km from the coast (Site 1 in Fig. 1), can contain upwelled water collected from either the western or the southern coast, or a combination of both.

Time series studies on the persistence and intensity of winds and upwelling events on the Portuguese western coast describe several and sometimes contradictory scenarios. For example, Bakun (1990), Casabella et al. (2014), Lorenzo et al. (2005), and Ramos et al. (2013) reported an enhancement of favourable conditions for upwelling in recent years but, in contrast, other authors report a weakening in the number and intensity of upwelling events with climate alterations (Alvarez et al., 2008; Álvarez Salgado et al., 2008; Alves and Miranda, 2012; Lemos and Pires, 2004; Lemos and Sansó, 2006).

## 2. Methods

### 2.1. Time series sources

Data for wind speed and direction were obtained from the Blended Daily Averaged 0.25-degree Sea Surface Winds (at 10 m level) product, provided by the National Oceanic and Atmospheric Administration (NOAA) and National Climatic Data Centers (Zhang et al., 2006). The SST time series for the Portuguese coast was extracted from the NOAA OI daily SST with a 0.25-degree resolution model (Reynolds et al., 2007).

Ekman transport was calculated following Bakun (1973) and Cropper et al. (2014). Latitudinal ($Q_x$) and longitudinal ($Q_y$) components of Ekman transport were considered to be the upwelling indices whereby negative values of $Q_x$ and $Q_y$, would indicate upwelling conditions along the western and southern coasts, respectively.

### 2.2. Time series analysis

A time series $\{Y_t\}_{t=1}^{N}$ is a collection of observations indexed by time $t$. In this study, time series were extracted for the period from 13th January 1988 to 31st December 2013, covering a time horizon of 26 years ($N =$ 9485 daily observations). Few missing observations were detected; in fact the longer interpolated lag was 5 days (0.97%). Where there were missing observations, estimation and imputation were performed with linear interpolation (R function na.interp() (Hyndman, 2015)). All the statistical analyses were performed using the R 3.2.2 software (R Core Team, 2015) and considered at a level of significance of 0.05.

#### 2.2.1. Time series modelling

Classical decomposition methods have been widely identified in the marine sciences literature (e.g. Loisel et al., 2014; Mélin et al., 2011;

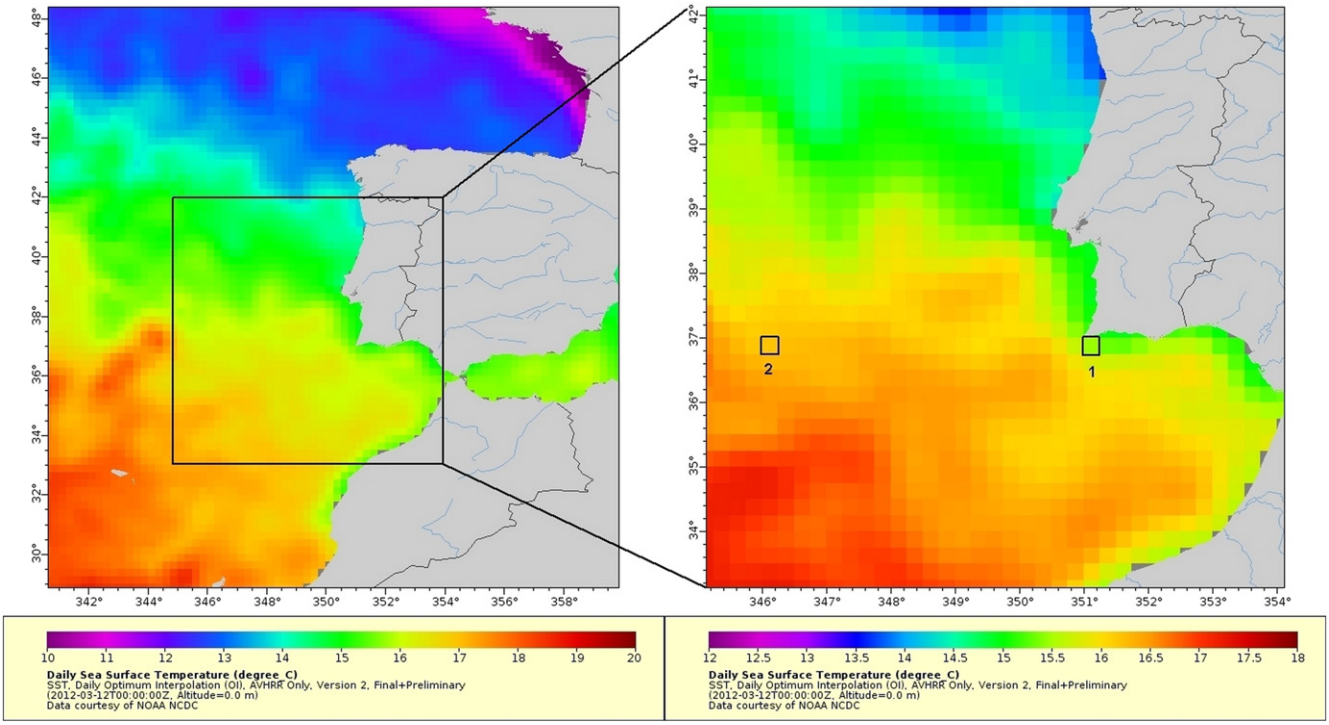


**Fig. 1.** Study area in upwelling conditions. Boxes 1 (study site) and 2 (5° latitude further west of the study site) are the pixels from where the data were extracted (data courtesy of NOAA NC DC).

Vantrepotte and Mélin, 2010). With these methods, a time series is described using the following components: a trend component ($T_t$), which consists of the underlying long-term direction over the time horizon; a seasonal component ($S_t$), which is a repetitive pattern over time; and an irregular component ($I_t$), which is the unexplained variation of the time series that is not attributed to trend or seasonality. An additive model $Y_t = T_t + S_t + I_t, t = 1, \ldots, N$ was chosen (see Section 3.1) to decompose the daily time series into these components.

The strong seasonality of some time series makes it difficult to measure their trend (DeLurgio, 1998). Therefore, identification of the seasonal pattern ($S_t$), is an essential step so that the seasonal variation, can be eliminated without affecting the trend. This new time series is given by $Y_t^* = Y_t - S_t = T_t + I_t, t = 1, \ldots, N$.

*2.2.2. Trend analysis*

The usual approach when considering trend analysis consists of an estimation of a linear model for the seasonally adjusted time series ($Y_t^*$) (Astor et al., 2013; Lima and Wethey, 2012; Nicastro et al., 2013), where the historical data have a stable behavior across the time horizon. The linear model, by including $t = 1, \ldots N$ as a predictor variable, is given by $Y_t^* = \beta_0 + \beta_1 t + \varepsilon_t$, where the $\beta_0$ is the intercept, $\beta_1$ is the regression coefficient or slope, and $\varepsilon_t$ is the random error.

However, some structural disturbances can be observed in the dynamic structure of the time series. These are known as structural breaks and are points in time at which statistical patterns change. According to Wang et al. (2014), the structural breaks on data series should not be ignored as they highlight those sections of the time horizon where the increases or decreases of the trend are more pronounced.

The current study applies the usual approach and also the structural breaks approach, which consists of detecting structural changes within the seasonally adjusted time series, and then adjusting a linear model to each segment. The R package strucchange (Zeileis et al., 2015) has been used to detect structural breaks in the seasonally adjusted time series, which tests for structural changes in linear regression models, estimating the number of segments ($m$) and the breakpoints $\{t_k^*\}_{k=1}^{m-1}$, minimizing the Bayesian information criterion (BIC) and the residual sum of squares (RSS). The results of these trend analyses are described in terms of warming (W) and cooling (C) periods, depending on the sign of the regression coefficient estimated within each segment.

*2.2.3. Cross-correlation analysis*

The cross-correlation is a function used to examine the relationship between two time series, to identify whether two stationary series may be related, with the same characteristics of the correlation coefficient. From Section 2.2.1, a time series model has been fitted to the original time series $Y_t$. The residuals obtained after fitting an appropriate model should look like "white noise" and so, exhibit a stationary behavior. The practical importance of cross-correlation values can be assessed by comparing their maximum values (highest peaks in the graphical representation). Moreover, a significant peak at lag $d$ ($d \neq 0$) indicates that one time series is related to the other when delayed by time $d$ (Chatfield, 2004).

*2.2.4. Spectral analysis*

The identification and interpretation of the periodic components of a time series are crucial to understand the dynamics of the underlying oceanographic mechanism (Palma et al., 2010). Spectral analysis is a frequency domain statistical method, useful to unmask hidden time frequency in the data. Considering a time series, the down-weighting frequencies are obtained and converted to a time domain periodicity. The highest frequency corresponds to the time frequency of the time series (in our case, 365 days approximately). The next level of frequencies reveals other meaningful time domain periodicities.

When performing spectral analysis (Chatfield, 2004; Wilson et al., 2016), the longer time series are preferred since those will include several repetitions of the time frequency. Therefore, this method was applied to a time series of 26 years of daily values, and the results used for the period of 4 years when the validation programme took place.

The existence of trends in a time series must be assessed before spectral analysis. If the trend is not removed, the results of the spectral

analysis are likely to be dominated by this variation, making any other effects difficult or impossible to observe (Chatfield, 2004).

In frequency domain analysis, regression is commonly used as the underlying statistical model. The model adjusted to the time series can be expressed as a sum of sine and cosine waves (harmonic model):

$$UI_t = m_t + \sum_k (A_k \sin(w_k t) + B_k \cos(w_k t)) + z_t;$$

where $UI_t$ is the value of the upwelling index at day $t$; $m_t$ is the trend, which includes a parameter for the constant term; k is the number of periodicities found; the Fourier frequencies $w_k$ corresponds to the periodicities found; $A_k$ and $B_k$ are the unknown coefficients associated to the sine-cosine waves at the periodicities found, and $z_t$ is the stationary component. The unknown parameters $m_t$, $A_k$ and $B_k$ were estimated by ordinary least squares. The harmonic model with the period equal to the highest frequency was fitted to the data, and the residuals were used to obtain the next frequency in the data.

## 3. Results

### 3.1. Preliminary SST and upwelling analysis

The time series used in this case study are represented in Fig. 2. SST time series exhibit a pronounced seasonal pattern (Fig. 2a), while $Q_x$ and $Q_y$ (Fig. 2b and c, respectively) exhibit a temporal variability that has a constant mean and a variance that does not seem to vary over the time horizon.

Analysis of the SST time series (Figs. 2a, and 3a) shows that the marked seasonal effect has an annual frequency. The period is considered to be 365.25 days due to the average length of a year, as well as allowing for leap years in the Gregorian calendar.

The monthly evolution of the SST (Fig. 3a) shows thermal amplitude around 3 °C with a minimum (~14 °C) in February/March, and amplitude around 5 °C with a maximum (~23 °C) in September. In contrast to SST, the upwelling indices, $Q_x$ and $Q_y$, show a low seasonal effect (Fig. 3b, c). A high presence of outliers is observed for almost all the months and so, a comparison was established using the median and the interquartile range (IQR). Table 1 shows the months where the upwelling indices $Q_x$ and $Q_y$ reached the highest and lowest values for the median and for the IQR dispersion measure. Based on Table 1, it can be observed that the month with the highest median value is also the one with the highest variability between the 25% percentile and 75% percentile (IQR). On the other hand, the lowest IQR values were observed in the months with lower medians.

The box and whisker plots for $Q_x$ and $Q_y$ have a higher variability during the winter and spring months over the 26 years, while they are much less variable during the summer months, aggregating around lower median values, in agreement with Table 1.

A strong seasonal pattern has been identified through the decomposition of the time series for SST. Fig. 4 (top panel) shows that the additive decomposition method is the correct choice as the magnitude of the seasonal fluctuations does not vary with the level along the time horizon.

#### 3.1.1. Trend analysis: usual approach

The trend analysis was performed with the de-seasonalized SST time series ($\hat{y}_t^{[]}$), as explained in Section 2.2.2. Fig. 5a, shows the seasonally adjusted time series plot over the time horizon (1988 to 2013), fitted with the linear trend line $\hat{y}_t^{[]} = 17.7 + 3.9 \times 10^{-5} t$ and with a statistically significant trend test ($p$_value < 2e−16). On the basis of the positive slope, an increase of 0.15 ± 0.01 °C per decade is observed for the SST.

To compare the coastal area with open-ocean and understand to what extent the increasing temperature trend is modified by coastal processes (such as upwelling), the same analysis is performed for the daily time series of SST, over the same time horizon, but extracted from an oceanic location at 5° longitude further west from the study site (Fig. 5c). The linear trend line fitted to the time series is $\hat{y}_t^{[]} = 18.3 + 5.5 \times 10^{-5} t$, and it has a statistically significant trend ($p$_value < 2e−16) of about 0.20 ± 0.01 °C increase per decade.

Regarding upwelling indices, the same linear adjustment is performed revealing significant decreasing trends along the 26 years. The linear models obtained are $\hat{y}_t^{[]} = -266.4 - 2.4 \times 10^{-2} t$ ($p$_value = $2.9 \times 10^{-16}$) for $Q_x$ (Fig. 5e), corresponding to a decrease of 84.01 ± 10.73 $m^3\ s^{-1}\ km^{-1}$ per decade; and $\hat{y}_t^{[]} = 1313.3 - 6.9 \times 10^{-3} t$ ($p$_value = 0.010) for $Q_y$ (Fig. 5f), corresponding to a decrease of 25.20 ± 9.72 $m^3\ s^{-1}\ km^{-1}$ per decade.

#### 3.1.2. Trend analysis: structural breaks approach

Previously, a linear model was fitted on the assumption that the data shows the same behavior along the time horizon, but direct observation of the time series shows changes in the dynamic structure, where the behavior is not homogeneous (see Fig. 5b, d). Applying the structural break concept to de-seasonalized SST ($\hat{y}_t^{[]}$), five optimal partitions of the data (m = 5 segments) are detected with four breakpoints (Fig. 5b) at observations $t_1^* = 2465$, $t_2^* = 3889$, $t_3^* = 5677$ and $t_4^* = 7412$, corresponding to break dates: 1994 (day no. 287), 1998 (day no. 250), 2003 (day no. 211) and 2008 (day no. 129). Linear regression models are estimated for each segment and shown in Table 2.

Three consecutive cooling periods have been observed from 1988 until July 2003, followed by two warming periods between July, 2003 and December 2013 (Fig. 5b).

In the oceanic region at 5° latitude further west, the same number of breaking points are detected (Fig. 5d), at observations $t_1^* = 2471$, $t_2^* = 4164$, $t_3^* = 5620$ and $t_4^* = 7067$, corresponding to break dates: 1994 (day no. 293), 1999 (day no. 159), 2003 (day no. 154) and 2007 (day no. 140). The linear adjustment within each segment to this time series is summarised in Table 3. Two cooling periods and three warming periods have been detected at break dates close to the ones found in the study site, although, the last warming trend period is not statistically significant (Table 3, in grey).

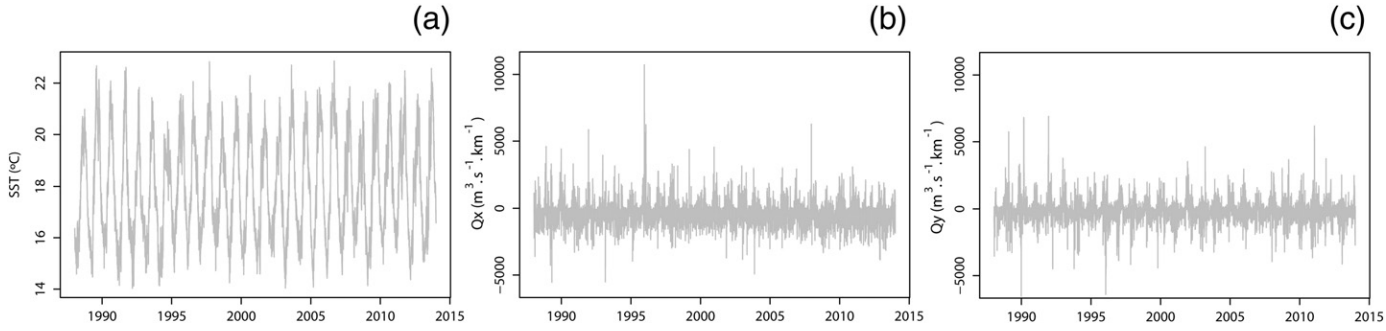


**Fig. 2.** Time series plot of (a) SST, (b) $Q_x$ and (c) $Q_y$.

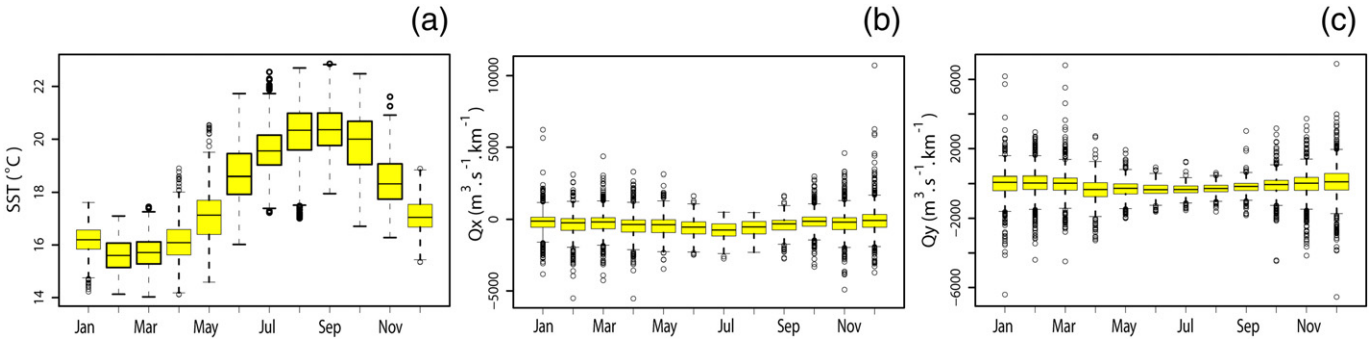


**Fig. 3.** The annual cycle by month of (a) SST and upwelling indices ((b) $Q_x$, (c) $Q_y$) by month.

Structural break analysis has also been applied to the upwelling indices $Q_x$ and $Q_y$ (not shown) and three breaking points are detected at approximately the same dates, in both time series. However, the majority of the linear adjustments within those segments are not statistically significant.

### 3.2. Relationship between Ekman transport components and SST

The relationship between Ekman transport and SST in the study area is well known (Fiúza, 1983; Loureiro et al., 2005; Relvas and Barton, 2002; Sousa and Bricaud, 1992). So, this knowledge should also be supported by the time series data and, if such a relationship exists, an indicator for lags could help to identify upwelling events. Therefore, a cross-correlation is used to examine and measure the relationship between the upwelling indices ($Q_x$ and $Q_y$) and SST. The residual time series is used, as the cross-correlation analysis should only be carried out with stationary time series. Fig. 6 shows the cross-correlation diagrams for $Q_x$ & SST and $Q_y$ & SST, respectively.

Statistically significant cross-correlations (highest peak) occur between $Q_x$ and SST ($r_{[Qx,SST]} = 0.17$) and between $Q_y$ and SST ($r_{[Qy,SST]} = 0.15$), with negative lags at 5 (Fig. 6a) and 2 (Fig. 6b) days, respectively. The positive sign for the cross-correlation coefficient confirms a direct relationship between the time series. As a check for a "casual" correlation between the time series, the cross-correlation analysis is also applied between each one of the upwelling indices and the SST data series extracted from the 5°W offshore site, where upwelling activity is not apparent. As expected, the oceanic site shows no significant cross-correlations between the time series for meaningful lags ($r_{[Qx,SST5°W]} = -0.08$, lag $= -797$; $r_{[Qy,SST5°W]} = -0.07$, lag $= -751$).

In conclusion, it is evident that the selection of the time series database is adequate and reflects the upwelling events in the study area, i.e., there is statistical evidence to state that favourable wind stress upwelling indices are followed by SST decreases at the Sagres coastal site.

### 3.3. Defining oceanographic seasons in the southwest coast of Portugal

After verifying the relationship between the upwelling indices ($Q_x$ and $Q_y$) with SST regimes at Sagres (previous section), it is now possible to use these data to infer the periodicity of upwelling events. Natural phenomena, such as upwelling, might have a frequency dependent variability and so, understanding this dependence may yield information about the underlying oceanographic mechanism. In this case study, spectral analysis has been applied to $Q_x$ and $Q_y$ time series, in order to find significant periodicities and thus delineate the oceanographic seasons based on upwelling forcing.

Results of the periodicities of the upwelling indices based on 26 years of daily $Q_x$ and $Q_y$ observations are able to highlight some significant cycles. In the case of $Q_x$, spectral analysis (Section 2.2.4) shows significant Fourier frequencies at 0.0027412, 0.0054823 and 0.0137059, corresponding to periodicities of 12 (~365 days), 6 (~182 days) and 2.5 (~73 days) months, respectively; while $Q_y$ shows dominant frequencies at 0.0027412 and 0.0059041, corresponding to periodicities of 12 (~365 days) and 6 (~169 days) months, respectively. In addition, Table 4 presents the estimates of the coefficients associated with the sine-cosine waves at the periodicities found, for both upwelling indices.

Considering the cross-correlation results (previous section) and the results for spectral analysis, the delineation between upwelling seasons becomes easier, especially when the time window is reduced to the 4 years sampled for the validation of remote sensing (Section 1.2). The $Q_x$ and $Q_y$ upwelling indices together with the SST over the reduced time series of 4 years are presented in Fig 7.

Given the periodicity found in $Q_x$ data series (periods of 2.5 months, close to the astronomical seasons calendar), four seasons with specific upwelling characteristics could be identified: summer (June, July, August) is characterised by an intense and persistent period with upwelling favourable conditions (negative $Q_x$), while autumn months (September, October, November) are the typical months with higher $Q_x$ values, indicating conditions favourable to relaxation of upwelling. In agreement, and according to the annual cycle of $Q_x$ (Fig. 3b), these are the seasons that show lower variability within the data. Winter months (December to February) show intermittent periods of negative $Q_x$, i.e. upwelling has been observed, especially in the winters of 2008–2009 and 2011–2012, but less pronounced in the other years. Spring months (March, April, May) of 2009, 2010 and 2012 have small but pronounced periods of negative $Q_x$. These observations are probably due to the high number of outliers observed in winter and spring months, in the annual cycle of $Q_x$ (Fig. 3b).

Regarding $Q_y$, the six months periodicity matches a favourable upwelling season from April till August where indices are persistently negative, and another season from September till March when upwelling conditions seem to be attenuated, although there are occasionally pronounced negative peaks, with an example in 2008–2009. This upwelling season is observable in the annual cycle of $Q_y$, by the lower median values for the referred months (Fig. 3c).

In the lowest panel (Fig. 7), there are several links between abrupt drops in the SST and favourable wind-stress periods, allowing identification of upwelling events. In summary, two marked seasons can be observed with contrasting features: summer, with persistent wind stress

**Table 1**
Robust descriptive statistics for the upwelling indices $Q_x$ and $Q_y$.

| | | Median value ($m^3\ s^{-1}\ km^{-1}$) | Month | IQR* ($m^3\ s^{-1}\ km^{-1}$) |
|---|---|---|---|---|
| $Q_x$ | Min | −741 | July | 847 |
| | Max | −81 | December | 905 |
| $Q_y$ | Min | −344 | June | 472 |
| | Max | 107 | December | 932 |

*IQR stands for interquartile range.

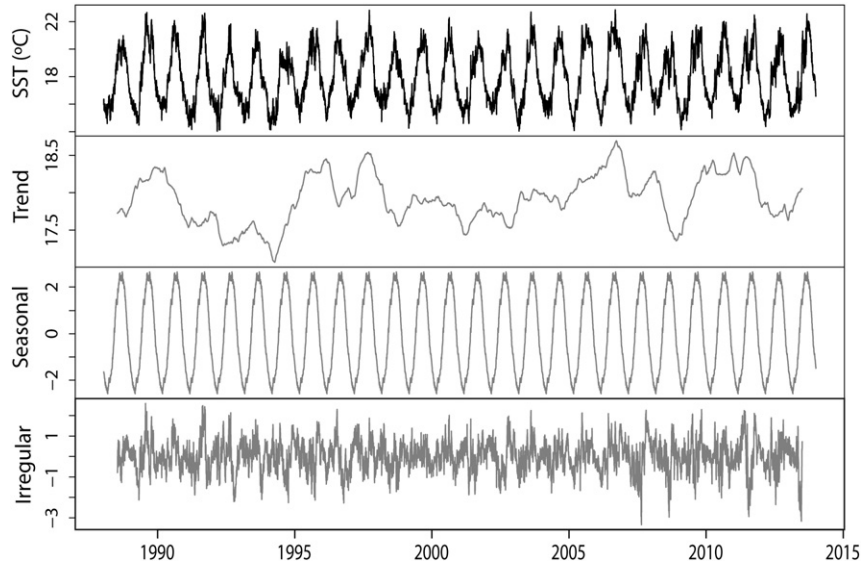


**Fig. 4.** Additive classical decomposition of SST.

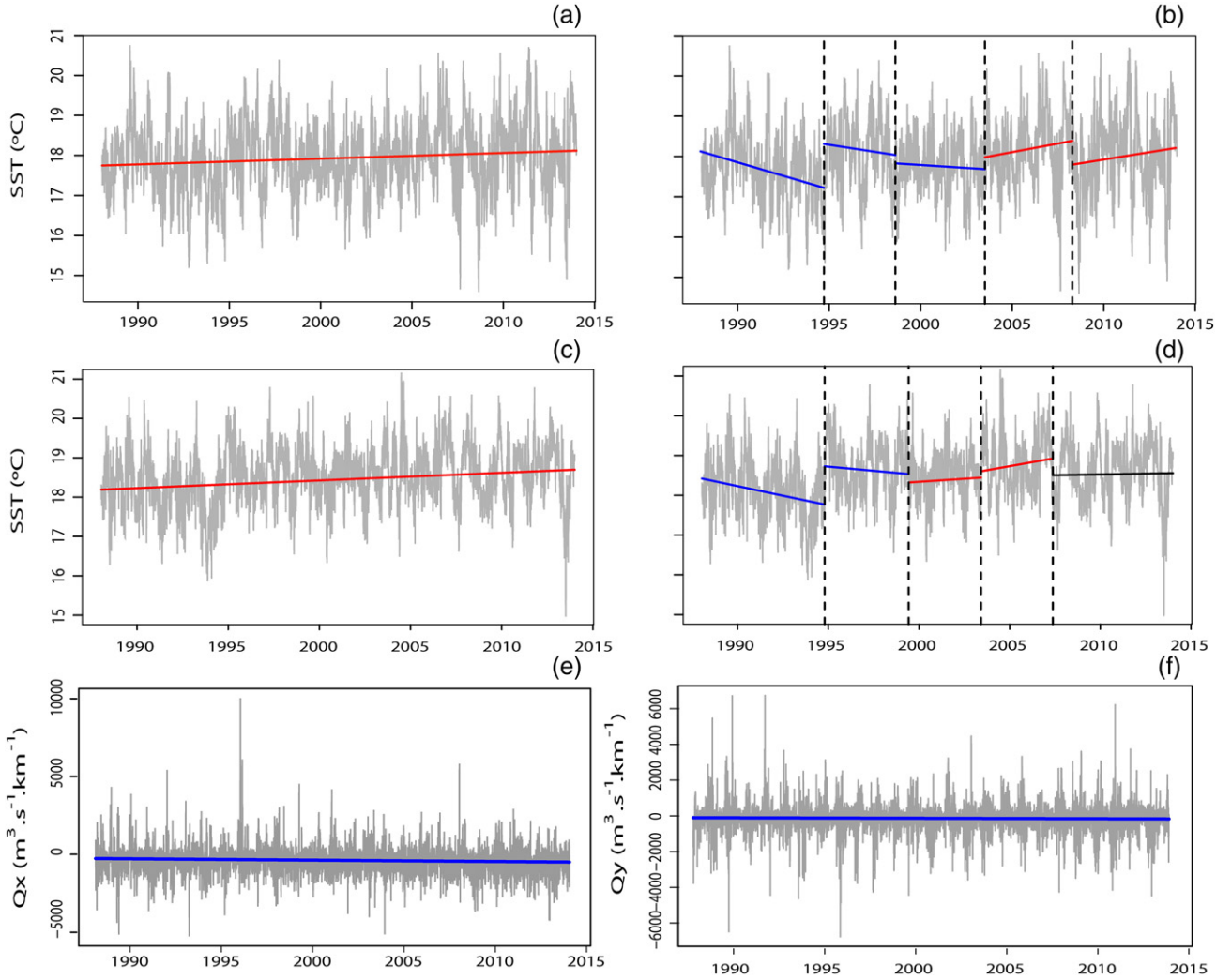


**Fig. 5.** Linear fit of the seasonally adjusted time series, and within each segment between breaking points: (a), (b) SST from Sagres coast; (c), (d) SST at a location 5° further west from Sagres coast. Linear adjustment of the seasonally adjusted time series (e) $Q_x$ and (f) $Q_y$.

**Table 2**
Linear adjustment by segments (study site, at Sagres coast).

| Period | Dates (from – to) | n | $\hat{\beta}_1$ | Std. error | *p*_value | ΔSST (°C per decade) |
|---|---|---|---|---|---|---|
| *C1 | January 1988–October 1994 | 2465 | $-3.67 \times 10^{-4}$ | $2.23 \times 10^{-5}$ | $\flat 2 \times 10^{-6}$ | −1.34 |
| C2 | October 1994–November 1998 | 1425 | $-1.94 \times 10^{-4}$ | $5.08 \times 10^{-5}$ | 0.0001 | −0.71 |
| C3 | November 1998–July 2003 | 1789 | $-7.80 \times 10^{-5}$ | $2.95 \times 10^{-5}$ | 0.0068 | −0.28 |
| *W1 | July 2003–May 2008 | 1745 | $2.34 \times 10^{-4}$ | $3.82 \times 10^{-5}$ | $\flat 2 \times 10^{-6}$ | 0.85 |
| W2 | May 2008–December 2013 | 2065 | $2.00 \times 10^{-4}$ | $3.48 \times 10^{-5}$ | $\flat 2 \times 10^{-6}$ | 0.73 |

* (C) and (W) stands for cooling and warming periods, respectively.

matches pronounced decreases in SST; and autumn, when relaxation of upwelling can be linked to increases in SST. Spring and winter seasons have higher interannual variability, characterised by occasional upwelling events, more intense in spring than in winter. 2009, 2010 and 2012 are years when upwelling events occur in spring, while in 2008/2009 and in 2011/2012 occasional upwelling events are apparent in winter.

## 4. Discussion

One focus of this study is the long-term trends (i.e. over one decade). In previous studies (Astor et al., 2013; Lima and Wethey, 2012; Nicastro et al., 2013), the researchers have investigated SST trends over a long time period using linear regression model. For example, Nicastro et al. (2013), have described an increase in SST of 0.2 °C per decade from 1982–2011 in southwestern Iberian Peninsula. Using the same database in a study from 1982, Lima and Wethey (2012), also mention an average increase of 0.27 °C per decade for the eastern Atlantic coast (around 0.2 °C for Sagres area); In these studies, the trend in SST data sets has the same dynamic rule for the temporal horizon. Using the same approach in our study, the increase in the SST in the study area is about 0.15 ± 0.01 °C per decade, showing slightly lower temperature values, but in the same order of magnitude of other studies performed in adjacent areas. This slight discrepancy could be explained by the different time horizon chosen for the study. Regarding the same analysis performed at an oceanic site, further away from coastal processes (about 555 km from the study site), the temperature increment is slightly higher. The lower rate of temperature increase near coast could be an indicator of the persistence of cold water masses in this region, probably due to upwelling processes (Fiúza et al., 1982; Goela et al., 2015; Loureiro et al., 2005, 2011). Nonetheless, the increase in temperature is observable even close to the coast, confirming warming trends in the area, when the entire time series over the 26 years is taken into account.

This study has also looked in more detail into the dynamics of the SST and wind stress based upwelling indices by applying structural breaks analysis to the time series. In the case of SST, the linear adjustments of the five segments between the four breaking points are statistically significant, supporting the idea that the changes within the dynamic structure should not be neglected. Indeed, the analyses of the temporal trends for SST in the 20th century have been reported as far from being uniform (deCastro et al., 2009). These trends are highly dependent on spatial and temporal scales, and it is possible to observe opposing trends at different time periods (IPCC, 2007). Such differences might arise from biogeophysical forcing, but also potentially due to differences in instruments and measurement methodology (Aguilar et al., 2003). Over the duration of the study period, 7 different spatial missions were launched with the AVHRR SST sensor type and one of the four breaking points in SST time series coincides approximately with changes in the satellite mission (i.e. launching of NOAA 14 in the end of 1994). Moreover, the breaking points in the study site are similar to those identified at the site 5° further west, which might indicate that these alterations could indeed come also from measurement methodology alterations, together with the biogeochemical forcing. Nonetheless, the structural breaks analysis at the two sites shows that there is a more marked increase in SST in this region of the Atlantic during the last decade (Fig. 5b, c).

Trend analysis was also applied to wind stress based upwelling indices, but in this case, structural breaks were not so evident. Linear modelling adjustment's reveal statistically significant decreasing trends (84.01 $m^3\ s^{-1}\ km^{-1}$ and 25.20 $m^3\ s^{-1}\ km^{-1}$ decrease per decade for $Q_x$ and $Q_y$, respectively) in upwelling indices along the time horizon, both in the west and in the south coasts. According to the definition (Section 2.1), negative $Q_x$ and $Q_y$ indicate offshore Ekman transport. Thus, results seem to indicate an increase in favourable conditions for upwelling along the Portuguese southwest coast, corroborating Bakun's (1990) work. However, an overall study of the upwelling phenomena, namely duration and intensity of each event, would be necessary to confirm this.

Cross-correlation is a measure of association between one time series and the past, present and future values of another time series. The statistically significant lagged correlations of 5 days between $Q_x$ and SST, and 2 days between $Q_y$ and SST suggest either: a) the re-establishment of a longshore flow, after wind relaxation, similar to the observations of Relvas and Barton (2002) or; b) a cause-effect relationship between wind favourable conditions (negative indices) and a decrease in SST values. The delayed response of SST to $Q_x$, relative to $Q_y$, might be explained by the upwelled filaments stimulated by northerly wind stress favourable conditions ($Q_x$), often originating further north and only reaching the study area after the persistence of upwelling conditions (Fiúza, 1983; Loureiro et al., 2005; Relvas and Barton, 2002; Sousa and Bricaud, 1992). Indeed, smaller lags between peaks of upwelling favourable winds and temperature anomalies have been observed at northerly located study sites (Oliveira et al., 2009).

The low values of the cross-correlation might be explained by the many other factors influencing SST (e.g. calendar seasons' succession, North Atlantic Oscillation (Greatbatch, 2000), El-Niño Southern Oscillation (Hertig et al., 2015)). Moreover, upwelling occurs as filaments with diverse orientations (Relvas and Barton, 2002), thus, it is not guaranteed that the Sagres study site is always significantly affected by these filaments, even though they are present in the surrounding area. To prove a direct relationship between SST and upwelling indices over the duration of a long time series is difficult, but analyses of isolated events at a specific study site demonstrate more clearly the effects of wind forcing on SST (Goela et al., 2015; Loureiro et al., 2005; Palma et al., 2010). From this base, a time window of interest was defined, coinciding with a major sampling campaign period for ocean colour remote sensing validation purposes, and $Q_x$, $Q_y$ and SST were plotted (Fig. 7). The comparison between datasets shows that $Q_x$ is the prominent index related to more pronounced and persistent upwelling events or seasons, that can be easily observed in the summers of 2009 and 2011, when significant temperature anomalies coincided with favourable wind-stress conditions along the west coast (Fig. 7). $Q_y$ forcing acted together with $Q_x$ in summer, corroborating previous studies in the area (Loureiro et al., 2005; Relvas and Barton, 2002; Sánchez and Relvas, 2003). These facts are also reflected in the annual cycles of upwelling indices (Fig. 3b and c, Table 1), where lower variability is observed in summer. However, although not often reported in the literature, the present study also shows some evidence for small upwelling events in winter

**Table 3**
Linear adjustment by segments (5° W from the study site at Sagres coast).

| Period | Dates (from–to) | n | $\hat{\beta}_1$ | Std. error | p_value | ΔSST (°C per decade) |
|---|---|---|---|---|---|---|
| C1 | January 1988–October 1994 | 2471 | $-2.725 \times 10^{-5}$ | $1.94 \times 10^{-5}$ | $<2 \times 10^{-6}$ | −0.10 |
| C2 | October 1994–June 1999 | 1694 | $-1.188. \times 10^{-4}$ | $3.102 \times 10^{-5}$ | $2 \times 10^{-4}$ | −0.43 |
| W1 | June 1999–June 2003 | 1457 | $8.556 \times 10^{-5}$ | $3.466 \times 10^{-5}$ | 0.0137 | 0.31 |
| W2 | June 2003–May 2007 | 1448 | $2.290 \times 10^{-5}$ | $4.298 \times 10^{-5}$ | $<2 \times 10^{-6}$ | 0.08 |
| – | May 2007–December 2013 | 2419 | $2.190 \times 10^{-4}$ | $2.096 \times 10^{-5}$ | 0.296 | 0.80 |

* (C) and (W) stand for warming cooling and warming periods, respectively.

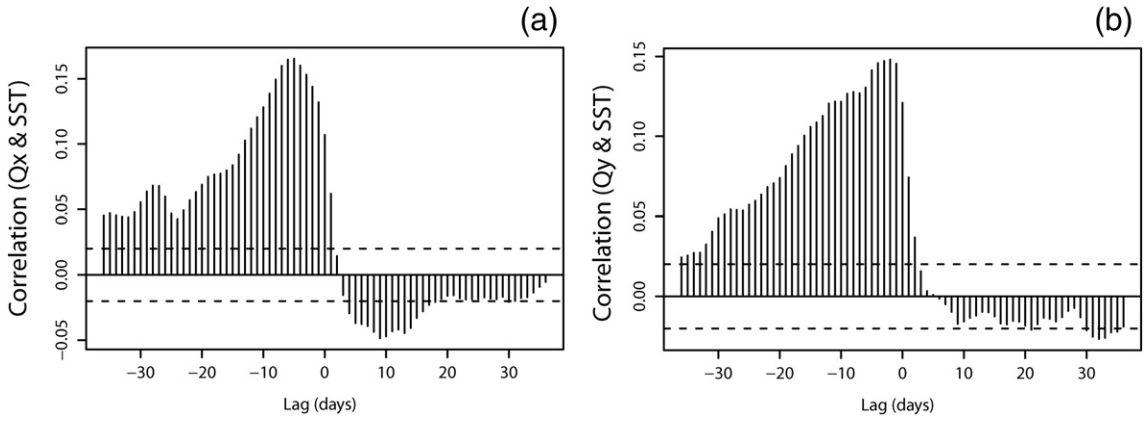


**Fig. 6.** Cross-correlation between (a) $Q_x$ and SST and (b) between $Q_y$ and SST (b).

months, stimulated mostly with favourable $Q_y$. These are rare and less pronounced (e.g. winter of 2008–2009, Fig. 7).

Although oceanographic seasons in other studies in the area have been basically divided into upwelling and non-upwelling periods (Loureiro et al., 2005, 2011; Relvas and Barton, 2002; Sánchez and Relvas, 2003), in this study, we propose a categorization of seasons based on the merging of the periodicity of upwelling wind stress indices and coincident calendar seasons. Summer is the season showing the most persistent and intense upwelling events, followed by spring. Autumn is the season showing the most signals for the relaxation of upwelling conditions, followed by winter, where only a few and short events were observed (2008–2009 and 2011–2012, where a decline from 16 °C to about 14 °C in the SST was observed), likely related to the short periods of strong winds during winter storms. In a study also based on spectral analysis of upwelling indices, performed in the western coast of Portugal, Palma et al. (2010) identified only three seasons of specific upwelling characteristics (4 months cycles). The difference from the present study is that Palma et al. (2010) were only working on the western coast and therefore did not need to account for related processes along the southern coast, such as upwelling forcing from westerly winds or a recurrent warm countercurrent flowing westwards (Loureiro et al., 2005; Relvas and Barton, 2002).

**Table 4**
Harmonic regression estimates for $Q_x$ and $Q_y$.

| Harmonic variables ($Q_x$) | Coefficient | p_value |
|---|---|---|
| Constant | −266.7 | $<2e^{-16}$ |
| t | −0.024 | $2.49e^{-16}$ |
| Sin (365 days period) | −61.5 | $5.51e^{-8}$ |
| Cos (365 days period) | 279.8 | $<2e^{-16}$ |
| Sin (182 days period) | −98.8 | $<2e^{-16}$ |
| Cos (182 days period) | −37.0 | 0.001 |
| Sin (73 days period) | −63.5 | $2.01e^{-8}$ |
| Cos (73 days period) | 64.0 | $1.53e^{-8}$ |
| **Harmonic variables ($Q_y$)** | **Coefficient** | **p_value** |
| Constant | −129.1 | $<2e^{-16}$ |
| t | −0.007 | 0.0057 |
| Sin (365 days period) | −39.63 | 0.0001 |
| Cos (365 days period) | 197.20 | $<2e^{-16}$ |
| Sin (169 days period) | −69.97 | $1.08e^{-11}$ |
| Cos (169 days period) | 38.98 | 0.0001 |

## 5. Conclusions

This study used the publically available NOAA database for both SST (Optimum Interpolation of daily SST from a 0.25-degree resolution model) and wind speed and direction (Blended Daily Averaged 0.25-degree Sea Surface Winds product). These data defined the oceanographic seasons by examining patterns and relationships in and between SST and upwelling indices off the coast of southwestern Iberia (Sagres) collected from 13th January 1988 to 31st December 2013, covering a time horizon of 26 years. This time horizon was sufficiently long to enable a reliable statistical analysis using statistical methodologies for dependent data to enable the identification of seasonality and periodicity for these events within a more localised time window from the end of 2008 till beginning of 2012, which was a period of intensive sampling at Sagres for validation of satellite sensors.

Preliminary analysis of the SST time series showed an increase of 0.15 °C per decade for SST over the duration of a 26 year time horizon; this was a slightly lower heating rate than suggested in other published data. Further offshore, this rate attained values close to 0.2 °C per decade. The lower increasing trend in the coastal site was probably related to upwelling processes in the coastal area. Structural break analysis also inferred that this increment was more significant during the last decade.

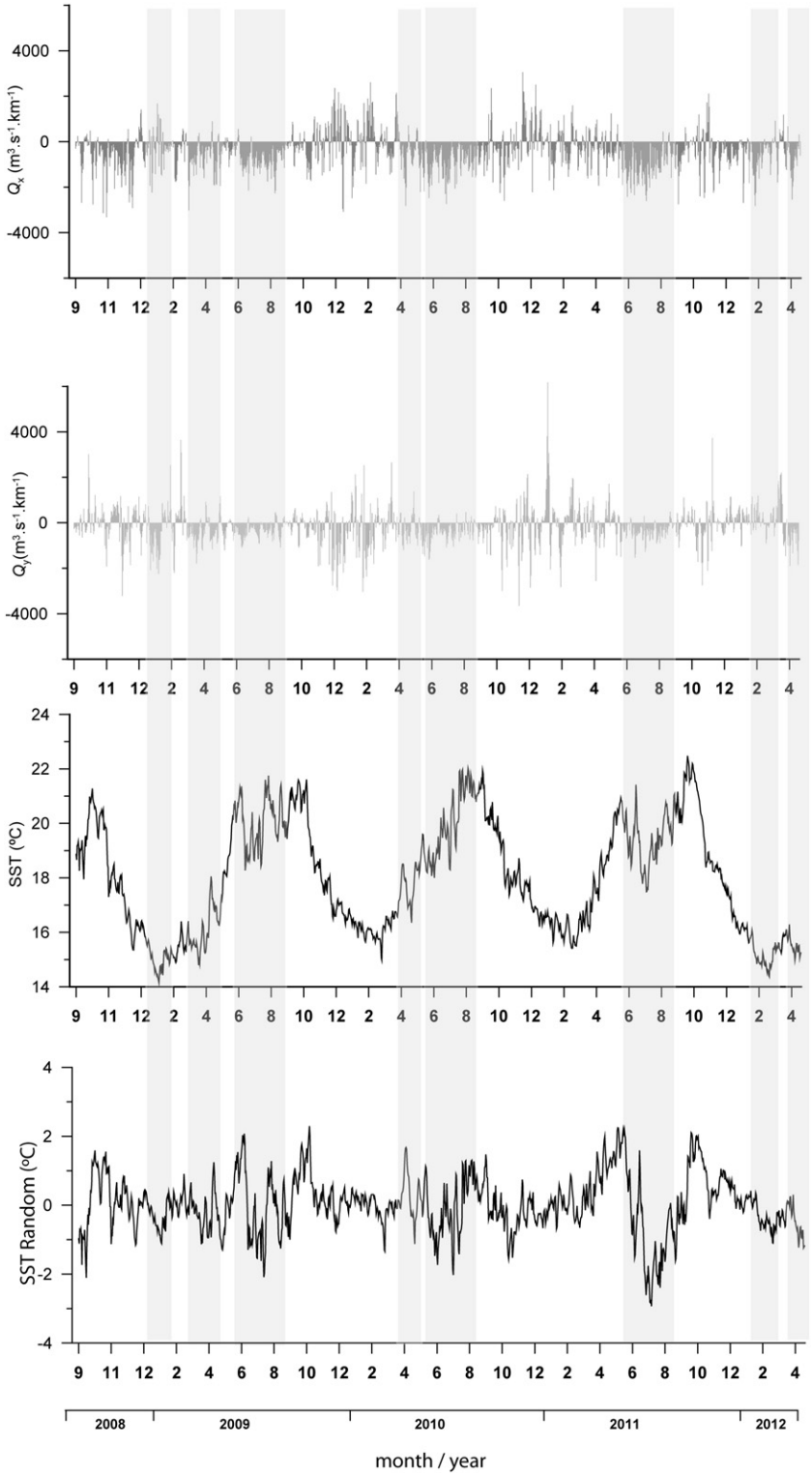


**Fig. 7.** Daily data on wind-stress based upwelling indices along west ($Q_x$) and south coast ($Q_y$), SST and the random component from SST (without trend and seasonality) from September 2008 to April 2012 (sampling campaign period for MERIS validation). Periods with visible correspondences between upwelling favourable wind stress conditions and SST drops are highlighted in grey.

The relationship between the wind stress forcing of upwelling and the abrupt decreases in SST along the Sagres coast corroborated the results obtained from previous studies on the area, showing the dominance of upwelling originating from northerly winds over westerly wind forcing. According to cross-correlation analysis, decreases in SST events seem to occur 5 days after persistent wind stress, favourable to upwelling in the west coast, and two days after persistent wind stress favourable to upwelling in the south coast. In agreement with previous studies, the delay in the response of SST to favourable $Q_x$ indices was attributed to the time that the upwelling filaments might take to reach the south coast after being upwelled on the west coast. This information is relevant to coastal management, including the aquaculture sector, enabling the forecasting of phytoplankton blooms after an upwelling event.

The relationship between wind forcing time series and SST time series was verified, with significant lags found between favourable upwelling indices and abrupt decreases in temperature. Results of the spectral analysis were applied to the localised time series for upwelling indices between 2008 and 2012, to help define the upwelling seasons in the study area. Four seasons were defined: summer (June, July, August), characterised by intense and persistent upwelling events; contrasting with autumn (September, October, November), with low upwelling activity; spring and winter presented higher interannual variability in terms of number and intensity of upwelling events, with spring marked by intense but limited periods of upwelling events. A proper definition of seasons in Sagres region, accounting for the characteristic upwelling regimes, would allow for a better selection and categorization of data for current and future studies in the area. For example, the parameterization of optical properties of the water column for remote sensing of ocean colour, or the study of the fate of upwelling filaments in the area, or even to characterise the region in terms of phytoplankton dynamics.

## Acknowledgements

P.C. Goela and S. Cristina were funded by PhD grants from FCT - Portugal (SFRH/BD/78356/2011 and SFRH/BD/78354/2011, respectively); research of C. Cordeiro was funded by FCT - Portugal, through the project UID/MAT/00006/2013. J.Icely was funded by EU FP7 AQUA_USER (grant agreement no. 607325), www.aqua-users.eu, and Horizon 2020 AquaSpace (grant no. 633476); S. Danchenko was funded by Erasmus Mundus EMJD MACOMA; A. Newton was funded by EU FP7 project DEVOTES (grant agreement no. 308392), www.devotes-project.eu.

The Authors thank the two Reviewers for their sound advice and helpful remarks on improvements for this article.

## References

Aguilar, E., Auer, I., Brunet, M., Peterson, T.C., Wieringa, J., 2003. Guidelines on climate metadata and homogenization. WMO/TD 1186. Organization, World Meteorological.

Álvarez Salgado, X., Labarta, U., Fernández-Reiriz, M., Figueiras, F., Rosón, G., Piedracoba, S., Filgueira, R., Cabanas, J., 2008. Renewal time and the impact of harmful algal blooms on the extensive mussel raft culture of the Iberian coastal upwelling system (SW Europe). Harmful Algae 7 (6), 849–855.

Alvarez, I., Gomez-Gesteira, M., deCastro, M., Dias, J.M., 2008. Spatiotemporal evolution of upwelling regime along the western coast of the Iberian Peninsula. J. Geophys. Res. Oceans 113 (C7).

Alves, J.M., Miranda, P.M., 2012. Variability of Iberian upwelling implied by ERA-40 and ERA-Interim reanalyses. Tellus A 65, 19245.

Astor, Y., Lorenzoni, L., Thunell, R., Varela, R., Muller-Karger, F., Troccoli, L., Taylor, G., Scranton, M., Tappa, E., Rueda, D., 2013. Interannual variability in sea surface temperature and $fCO_2$ changes in the Cariaco Basin. Deep-Sea Res. II Top. Stud. Oceanogr. 93, 33–43.

Bakun, A., 1973. Coastal upwelling indices, west coast of North America. Tech. Rep. Technical Report NMFS SSRF-671. NOAA.

Bakun, A., 1990. Global climate change and intensification of coastal ocean upwelling. Science 247, 198–201.

Banzon, V., Reynolds, R. and National Center for Atmospheric Research Staff (Eds), last modified 9 June 2016. The Climate Data Guide: SST data: NOAA Optimal Interpolation (OI) SST Analysis, version 2 (OISSTv2) 1x1, https://climatedataguide.ucar.edu/climate-data/sst-data-noaa-optimal-interpolation-oi-sst-analysis-version-2-oisstv2-1x1.

Casabella, N., Lorenzo, M., Taboada, J., 2014. Trends of the Galician upwelling in the context of climate change. J. Sea Res. 93, 23–27.

Chatfield, C., 2004. The Analysis of Time Series. An Introduction. sixth ed. Chapman & Hall, Florida, USA.

Costoya, X., deCastro, M., Gómez-Gesteira, M., Santos, F., 2015. Changes in sea surface temperature seasonality in the Bay of Biscay over the last decades (1982–2014). J. Mar. Syst. 150, 91–101.

Cristina, S., Goela, P., Icely, J., Newton, A., Fragoso, B., 2009. Assessment of water-leaving reflectance of oceanic and coastal waters using MERIS satellite products off the southwest coast of Portugal. J. Coast. Res. SI 56, 1479–1483.

Cristina, S.C.V., Moore, G.F., Goela, P.R.F.C., Icely, J.D., Newton, A., 2014. In situ validation of MERIS marine reflectance off the southwest Iberian Peninsula: assessment of vicarious adjustment and corrections for near-land adjacency. Int. J. Remote Sens. 35 (6), 2347–2377.

Cristina, S., Icely, J., Goela, P., DelValls, T., Newton, A., 2015. Using remote sensing as a support to the implementation of the European Marine Strategy Framework Directive in SW Portugal. Cont. Shelf Res. 108, 169–177 (October).

Cropper, T.E., Hanna, E., Bigg, G.R., 2014. Spatial and temporal seasonal trends in coastal upwelling off Northwest Africa, 1981–2012. Deep-Sea Res. I Oceanogr. Res. Pap. 86, 94–111.

deCastro, M., Gómez-Gesteira, M., Alvarez, I., Gesteira, J., 2009. Present warming within the context of cooling–warming cycles observed since 1854 in the Bay of Biscay. Cont. Shelf Res. 29 (8), 1053–1059.

DeLurgio, S.A., 1998. Forecasting Principles and Applications. Statistical & Probability, McGraw-Hill, USA.

Fiúza, A., 1983. Coastal upwelling: its sedimentary record. Part A. Responses of the Sedimentary Regime to Present Coast Upwelling. Ch. Upwelling patterns off Portugal, Plenum, New York, pp. 85–98.

Fiúza, A.F.G., Macedo, M.A., Guerreiro, M.R., 1982. Climatological space and time variations of the Portuguese coastal upwelling. Oceanol. Acta 5, 31–40.

Girondot, M., Kaska, Y., 2015. Nest temperatures in a loggerhead nesting beach in Turkey is more determined by sea surface than air temperature. J. Therm. Biol. 47, 13–18.

Goela, P.C., Icely, J., Cristina, S., Newton, A., Moore, G., Cordeiro, C., 2013. Specific absorption coefficient of phytoplankton off the southwest coast of the Iberian Peninsula: a contribution to algorithm development for ocean colour remote sensing. Cont. Shelf Res. 52, 119–132.

Goela, P., Danchenko, S., Icely, J., Lubian, L., Cristina, S., Newton, A., 2014. Using CHEMTAX to evaluate seasonal and interannual dynamics of the phytoplankton community off the south-west coast of Portugal. Estuar. Coast. Shelf Sci. 151, 112–123.

Goela, P.C., Icely, J., Cristina, S.C.V.C., Danchenko, S., DelValls, T.A., Newton, A., 2015. Using bio-optical parameters as a tool for detecting changes in the phytoplankton community (SW Portugal). Estuar. Coast. Shelf Sci. 167, 125–137.

Greatbatch, R.J., 2000. The North Atlantic oscillation. Stoch. Env. Res. Risk A. 14 (4+5), 213–242 (213–242).

Hansen, J., Ruedy, R., Sato, M., Lo, K., 2010. Global surface temperature change. Rev. Geophys. 48 (4).

Haynes, R., Barton, E.D., Pilling, I., 1993. Development, persistence, and variability of upwelling filaments off the Atlantic coast of the Iberian Peninsula. J. Geophys. Res. 98, 22681–22692 (December).

Hertig, E., Beck, C., Wanner, H., Jacobeit, J., 2015. A review of non-stationarities in climate variability of the last century with focus on the North Atlantic–European sector. Earth Sci. Rev. 147, 1–17.

Hyndman, R.J., 2015. Forecast: Forecasting functions for time series and linear models. R Package Version 5.9.

IPCC, 2007. Climate Change 2007: The Physical Science Basis, Contribution of Working Group I to the Fourth Assessment Report of the Intergovernmental Panel on Climate Change. Cambridge University Press, Cambridge, United Kingdom and New York, NY, USA (996 pp.).

Khalil, I., Atkinson, P.M., Challenor, P., 2016. Looking back and looking forwards: historical and future trends in sea surface temperature (SST) in the Indo-Pacific region from 1982 to 2100. Int. J. Appl. Earth Obs. Geoinf. 45 (Part A), 14–26.

Lemos, R.T., Pires, H.O., 2004. The upwelling regime off the West Portuguese Coast, 1941–2000. Int. J. Climatol. 24 (4), 511–524.

Lemos, R.T., Sansó, B., 2006. Spatio-temporal variability of ocean temperature in the portugal current system. J. Geophys. Res. Oceans 111 (C4).

Lima, F.P., Wethey, D.S., 2012. Three decades of high-resolution coastal sea surface temperatures reveal more than warming. Nat. Commun. 3 (704) (February).

Liu, Y., Minnett, P.J., 2015. Evidence linking satellite-derived sea-surface temperature signals to changes in the Atlantic meridional overturning circulation. Remote Sens. Environ. 169, 150–162.

Lluch-Cota, S.-E., 2000. Coastal upwelling in the eastern Gulf of California. Oceanol. Acta 23 (6), 731–740.

Loisel, H., Mangin, A., Vantrepotte, V., Dessailly, D., Dinh, D.N., Garnesson, P., Ouillon, S., Lefebvre, J.-P., Mériaux, X., Phan, T.M., 2014. Variability of suspended particulate matter concentration in coastal waters under the Mekong's influence from ocean color (MERIS) remote sensing over the last decade. Remote Sens. Environ. 150 (0), 218–230.

Lorenzo, E.D., Miller, A., Schneider, N., McWilliams, J., 2005. The warming of the California Current System: dynamics and ecosystem implications. J. Phys. Oceanogr. 35, 336–362.

Loureiro, S., Newton, A., Icely, J., 2005. Microplankton composition, production and upwelling dynamics in Sagres (SW Portugal) during the summer of 2001. Sci. Mar. 69 (3), 323–341.

Loureiro, S., Reñé, A., Garcés, E., Camp, J., Vaqué, D., 2011. Harmful algal blooms (HABs), dissolved organic matter (DOM), and planktonic microbial community dynamics at a near-shore and a harbour station influenced by upwelling (SW Iberian Peninsula). J. Sea Res. 65 (4), 401–413.

Marullo, S., Santoleri, R., Ciani, D., Borgne, P.L., Péré, S., Pinardi, N., Tonani, M., Nardone, G., 2014. Combining model and geostationary satellite data to reconstruct hourly SST field over the Mediterranean Sea. Remote Sens. Environ. 146, 11–23.

Mélin, F., Vantrepotte, V., Clerici, M., D'Alimonte, D., Zibordi, G., Berthon, J.F., Canuti, E., 2011. Multi-sensor satellite time series of optical properties and chlorophyll-*a* concentration in the Adriatic Sea. Prog. Oceanogr. 91 (3), 229–244 (November).

Narayan, N., Paul, A., Mulitza, S., Schulz, M., 2010. Trends in coastal upwelling intensity during the late 20th century. Ocean Sci. 6 (3), 815–823.

Nicastro, K.R., Zardi, G.I., Teixeira, S., Neiva, J., Serrão, E.A., Pearson, G.A., 2013. Shift happens: trailing edge contraction associated with recent warming trends threatens a distinct genetic lineage in the marine macroalga *Fucus vesiculosus*. BMC Biol. 11 (6) (January).

Oliveira, P.B., Nolasco, R., Dubert, J., Moita, T., Peliz, Á., 2009. Surface temperature, chlorophyll and advection patterns during a summer upwelling event off central Portugal. Cont. Shelf Res. 29 (5–6), 759–774.

Palma, S., Mouriño, H., Silva, A., Barão, M.I., Moita, M.T., 2010. Can *Pseudo-nitzschia* blooms be modeled by coastal upwelling in Lisbon Bay? Harmful Algae 9, 294–303.

Pauly, D., Christensen, V., 1994. Primary production required to sustain global fisheries. Nature 374, 255–257 (March).
Price, J., Weller, R., Schudlich, R., 1987. Wind-driven ocean ccurrent and Ekman transport. Science 238, 1534–1538.
R Core Team, 2015. R: A Language and Environment for Statistical Computing. R Foundation for Statistical Computing, Vienna, Austria.
Ramos, A.M., Pires, A.C., Sousa, P.M., Trigo, R.M., 2013. The use of circulation weather types to predict upwelling activity along the western Iberian Peninsula coast. Cont. Shelf Res. 69, 38–51.
Relvas, P., Barton, E., 2002. Mesoscale patterns in the Cape São Vicente (Iberian Peninsula) upwelling region. J. Geophys. Res. Oceans 107, 3164.
Reynolds, R., Smith, T., Liu, C., Chelton, D., Casey, K., Schlax, M., 2007. Daily high-resolution blended analyses for sea surface temperature. J. Clim. 20, 5473–5496.
Sánchez, R.F., Relvas, P., 2003. Spring–summer climatological circulation in the upper layer in the region of Cape St. Vincent, Southwest Portugal. ICES J. Mar. Sci. 60 (6), 1232–1250.
Schwing, F.B., O'Farrell, M., Steger, J.M., Baltz, K., 1996. Coastal upwelling indices — West Coast of North America 1946–95. Technical Memorandum NMFS NOAA-TM-NMFS-SWFSC-231. NOAA.
Singh, R.K., Maheshwari, M., Oza, S.R., Kumar, R., 2013. Long-term variability in Arctic sea surface temperatures. Polar Sci. 7 (3–4), 233–240.
Sousa, F.M., Bricaud, A., 1992. Satellite-derived phytoplankton pigment structures in the Portuguese upwelling area. J. Geophys. Res. Oceans 97 (C7), 11343–11356. http://dx.doi.org/10.1029/92JC00786.
Sousa, F.M., Nascimento, S., Casimiro, H., Boutov, D., 2008. Identification of upwelling areas on sea surface temperature images using fuzzy clustering. Remote Sens. Environ. 112 (6), 2817–2823.
Trenberth, K., Jones, P., Ambenje, P., Bojariu, R., Easterling, D., Tank, A.K., Parker, D., Rahimzadeh, F., Renwick, J., Rusticucci, M., Soden, B., Zhai, P., 2007. Climate Change 2007: The Physical Science Basis. Contribution of Working Group I to the Fourth Assessment Report of the Intergovernmental Panel on Climate Change. Cambridge University Press, Cambridge, United Kingdom and New York, NY, USA, Ch. Observations: Surface and Atmospheric Climate Change, pp. 235–335.
Vantrepotte, V., Mélin, F., 2010. Temporal variability in SeaWiFS derived apparent optical properties in European seas. Cont. Shelf Res. 30, 319–334.
Vantrepotte, V., Mélin, F., 2011. Inter-annual variations in the SeaWiFS global chlorophyll *a* concentration (1997–2007). Deep-Sea Res. I Oceanogr. Res. Pap. 58 (4), 429–441.
Wang, B., Sun, J., Motter, A.E., 2014. Detecting structural breacks in seasonal time series by regularized optimization. In: Deodatis, G., Ellingwood, B.R., Frangopol, D.M. (Eds.), Safety, Reliability, Risk and Life-Cycle Performance of Structures and Infrastructures. No. 978-1-315-88488-2. CRC Press, pp. 3621–3628.
Wilson, G., Reale, M., Haywood, J., 2016. Models for dependent time series. Monographs on Statistics an Applied Probability. CRC Press, Florida, New York, USA, London, UK.
Wooster, W., Bakun, A., McLain, D., 1976. The seasonal upwelling cycle along the eastern boundary of the North Atlantic. J. Mar. Res. 34 (2), 131–141.
Zeileis, A., Leisch, F., Hornik, K., Kleiber, C., 2015. strucchange: an R package for testing for structural change in linear regression models. R Package version 1.5–0.
Zhang, H.-M., Reynolds, R.W., Bates, J.J., 2006. Blended and gridded high resolution global sea surface wind speed and climatology from multiple satellites: 1987–present. American Meteorological Society 2006 Annual Meeting, Paper P2.23, Atlanta, GA, January 29–February 2, 2006.